PHYSICAL REVIEW B VOLUME 21, NUMBER 8 15 APRIL 1980

Angle-resolved photoemission, valence-band dispersions $E(\vec{k})$, and electron and hole lifetimes for GaAs

T.-C. Chiang, J. A. Knapp,* M. Aono,† and D. E. Eastman
IBM Thomas J. Watson Research Center, Yorktown Heights, New York 10598
(Received 3 December 1979)

Accurate valence-band dispersions $E(\vec{k})$ along the major symmetry directions Γ-K-X, Γ-Δ-X, and Γ-Λ-L have been determined for GaAs using simple angle-resolved photoemission techniques of general utility with synchrotron radiation for $25 \leq h\nu \leq 100$ eV. At these photon energies, emission features can be understood within the direct-transition model, and spectral peaks can be classified roughly into two categories: one being those associated with primary cone emission with a lifetime-broadened free-electron-like final-state dispersion, and the other (usually weaker) being those associated with secondary cone-surface umklapp emission which emphasizes valence-band critical points with high state densities. Valence-band dispersions $E(\vec{k})$ along the Γ-K-X symmetry line perpendicular to the surface are determined using normal-emission spectra (primary cone peaks) from the (110) surface at various photon energies. Valence-band dispersions $E(\vec{k})$ along Γ-K-X, Γ-Δ-X, and Γ-Λ-L symmetry lines parallel to the surface are determined using off-normal emission spectra (primary cone peaks) from the same (110) surface with fixed perpendicular component of the electron momentum $\hbar\vec{k}_\perp$ at a zone center (extended-zone scheme) and varying parallel component of the electron momentum $\hbar\vec{k}_\parallel$, which are obtained by suitably varying $h\nu$ and emission angles. Experimental valence-band dispersions and critical points are compared with other theoretical and experimental results. Simple formulas are derived to relate the widths of spectral peaks to electron and hole lifetimes. Initial hole lifetimes at valence critical points and typical final electron lifetimes are obtained. The latter yields final-state momentum broadenings (typically $\lesssim 10\%$ of the Brillouin-zone size) which are consistent with the direct-transition model.

I. INTRODUCTION

Angle-resolved photoemission from single crystals is now being widely used for determining the electronic band structure of solids.[1-14] Previous work on metals has demonstrated the capability and success of such techniques;[2-8] band dispersions $E(\vec{k})$ and lifetime broadening have been determined in certain cases. For semiconductors, despite numerous reported studies,[9-12] in most cases only rather limited information about band dispersions has been obtained. In particular, GaAs, being technologically important, has attracted much attention and is a model system for photoemission studies. In a previous short communication,[13] we determined the experimental band dispersions of GaAs along the Γ-K-X symmtery direction using simple photoemission techniques. In the present paper, we extend these studies and present detailed experimental techniques and results for GaAs. Specifically, we discuss experimentally measured valence-band dispersions $E(\vec{k})$ along all three major symmetry directions Γ-K-X, Γ-Δ-X, and Γ-Λ-L, and valence-hole and conduction-electron lifetimes. Our objective is twofold: (i) to give a relatively more complete one-electron description for GaAs from experimental measurements, and (ii) to illustrate the usefulness and success of such techniques which are of general utility for many materials.

In order to determine the valence-band dispersions from photoemission data, it is usually necessary to know the final-state band dispersions. At lower photon energies, a few methods,[5-8] most invoking theoretical interpolation, have been devised to obtain $E(\vec{k})$ dispersions using the direct-transition model and taking advantage of the fact that only a small number of final bands are involved. In most cases, $E(\vec{k})$ dispersions have been obtained for a limited range of $\vec{k}$ values, e.g., along one or two lines in $\vec{k}$ space. It is clearly desirable to determine the complete valence $E(\vec{k})$ dispersions, which can be done using a wider range of photon energies. The number of final bands becomes very large at higher energies and the problem is seemingly complex. However, our studies for GaAs show that,[13] helped by lifetime broadening of the final states at higher energies (say, $h\nu \gtrsim 25$ eV), angle-resolved photoemission spectra can be mainly described using quasi-free-electron primary cone emission and secondary cone-surface umklapp emission.[15] Intuitively, the crystal potential is a small perturbation at higher energies, and a nearly-free-electron approximation for the final states might be expected to work. This approximation has been applied before[2-4] to Cu and has yielded[2] rather accurate valence-band dispersions. Further attempts using free-electron plane-wave states to calculate the matrix elements and transition probabilities have not been very

successful,[3] and such procedures are not warranted since final-state wave functions are not simple plane waves. Here, we illustrate in simple terms how well the final band dispersions may be approximated by the nearly-free-electron dispersions, using a nonlocal pseudopotential band calculation.[16] Only qualitative statements will be made for the relative photoemission intensities, since this problem requires detailed realistic final-state wave functions. Invoking such final bands with lifetime-broadened free-electron-like dispersions for primary cone emission, we use simple techniques to map out the valence-band dispersions of GaAs. Valence-band dispersions $E(\vec{k})$ along the Γ-K-X symmetry line perpendicular to the surface are determined using normal-emission spectra from the (110) surface at various photon energies. Valence-band dispersions $E(\vec{k})$ along Γ-K-X, Γ-Δ-X, and Γ-Λ-L symmetry lines parallel to the surface are determined using off-normal-emission spectra by scanning the parallel component of the electron momentum $\hbar\vec{k}_{\parallel} = \hbar\vec{k} - \hbar\vec{k}_{\perp}$ along these symmetry lines (Γ-K-X, Γ-Δ-X, and Γ-Λ-L) parallel to the surface while holding $\hbar\vec{k}_{\perp}$ constant at the zone center (extended-zone scheme). This is achieved by suitably scanning both the polar emission angle and the photon energy simultaneously. The results obtained using these two methods for different but equivalent $\vec{k}$ points in the extended zone agree very well. We note that these techniques, or variations of them, have been used previously, e.g., for noble metals.[2-5] However, their applicability to compound semiconductors has only recently been demonstrated,[13] mainly due to an extended range of photon energies. Studies have been reported[9-11] in which the indirect transition model or the "one-dimensional density-of-states model" was used. As shown by this study of GaAs as well as work on other compound materials,[13,14,17] we conclude that generally, rather than exceptionally, the direct-transition model is the correct basis for understanding the photoemission results.

The widths of the transitions observed in the spectra are determined by band dispersions $E(\vec{k})$ and electron and hole lifetimes. Some specific examples of extracting electron and hole lifetimes from photoemission data have been described.[2,6,7] Here, we present rather general formulas and illustrate systematic methods for obtaining electron and hole lifetimes. In particular, valence-band hole lifetimes of GaAs are obtained at critical points. The experimental final-state electron lifetime yields a mean free path in agreement with previous estimates based on overlayer methods.[18] Consideration of broadening due to such lifetimes indicates that momentum uncertainty $\Delta\hbar k_{\perp}$ in photoemission is typically less than 10% of the Brillouin-zone size, consistent with a direct-transition picture.

The organization of this paper is as follows: A brief description of the experiment is given in Sec. II. An explanation of photoemission spectral features in terms of primary cone emission and secondary cone-surface umklapp emission is given in Sec. III, and the basic formulas are derived. Experimental data and valence-band dispersions $E(\vec{k})$ are presented and discussed in Sec. IV. Section V deals with electron and hole lifetimes, and finally, Sec. VI concludes the present treatment.

II. EXPERIMENTAL

GaAs has the fcc zinc-blende crystal structure with a lattice constant $a = 5.65$ Å; the cleavage plane is $\{110\}$. The main symmetry directions are $[110](\Gamma$-K-$X)$, $[100](\Gamma$-Δ-$X)$, $[111](\Gamma$-Λ-$L)$, and their equivalent directions; a picture of the Brillouin zone with the critical points can be found in standard textbooks.[19] The important dimensions of the Brillouin zone are: $\Gamma KX = \sqrt{2}\,(2\pi/a) = 1.57$ Å^{-1}, $\Gamma\Delta X = 2\pi/a = 1.11$ Å^{-1}, and $\Gamma\Lambda L = (\frac{3}{4})^{1/2}(2\pi/a) = 0.965$ Å^{-1}. The samples used were lightly Zn-doped p-type single crystals that were cleaved in an ultrahigh vacuum ($\sim 1\times 10^{-10}$ Torr) experimental chamber to expose the (110) face; and were measured at room temperature.

The experiments were done at the University of Wisconsin at Madison 240-MeV storage ring, with the synchrotron radiation monochromatized by a toroidal grating monochromator as the light source. A cylindrical mirror analyzer with 4° (full angle) angular resolution was used. The overall instrumental energy resolution was ~0.2 eV at the lower photon energies of ~25 eV, and decreased to ~0.5 eV by 100 eV. The light was incident at 45° with respect to the surface normal. Due to mechanical constraints of the system, the polarization of the light relative to the sample was determined in most cases by the collecting angles and cound not be adjusted freely. In general, configurations were chosen such that the electric field vector of the light had comparable magnitudes for the parallel and perpendicular components relative to the sample $(1\bar{1}0)$ mirror plane. With this mixed polarization, all valence-band states that are excited with s or p polarization contribute to the spectra.[20,21] This poses no difficulty in the following analysis since primary emission peak positions and line shapes, rather than absolute intensities, are of prime concern.

III. THEORY

A. Basic formulas

We consider the case of nearly-free-electron final states for the direct-transition model. The final Bloch states are then described by a free-electron-like dispersion.[13]

$$E_f(\vec{k}) = \hbar^2 |\vec{k}|^2/2m + E_0 = \hbar^2(k_\parallel^2 + k_\perp^2)/2m + E_0 , \quad (1)$$

where $\vec{k} = \vec{k}_\parallel + \vec{k}_\perp$, $\vec{k}_\parallel$ and $\vec{k}_\perp$ are the electron momentum components parallel and perpendicular to the surface defined in the extended zone scheme, respectively, and E_0 is the calculated "bottom of the muffin tin" referenced to the valence-band maximum E_v ($E_0 = -9.34$ eV for GaAs).[16] The justification for using Eq. (1) and the limitations due to lifetime broadening, etc. will be discussed later in this section. With energy conservation and momentum conservation (direct transitions).

$$E_f(\vec{k}) = E_i(\vec{k}) + h\nu , \quad (2)$$

where $E_i(\vec{k})$ is the initial Bloch-state energy referenced to E_v and $h\nu$ is the photon energy. The experimentally measured photoelectron kinetic energy E_k (referenced to the vacuum level) is related to E_f by

$$E_f = E_k + e\Phi , \quad (3)$$

where $e\Phi = 5.15$ eV is the measured photothreshold (vacuum level minus E_v) for GaAs. From Eqs. (1)–(3), simple kinematic equations can be derived:

$$\hbar k_\parallel = (2mE_k)^{1/2} \sin\theta \quad (4a)$$

$$= [2m(E_i + h\nu - e\Phi)]^{1/2} \sin\theta \quad (4b)$$

and

$$\hbar k_\perp = [2m(E_k \cos^2\theta - V_0)]^{1/2} \quad (5a)$$

$$= \{2m[(E_i + h\nu - e\Phi)\cos^2\theta - V_0]\}^{1/2} , \quad (5b)$$

where θ is the polar emission angle and $V_0 = E_0 - e\Phi = -14.5$ eV for GaAs is the inner potential (energy of the "bottom of the muffin tin" referenced to the vacuum level). From measured values of E_i for the interband transition at a selected $h\nu$ and polar angle θ, $\vec{k}$ is simply determined from Eqs. (4b) and (5b) to yield $E_i(\vec{k})$. For normal emission ($\theta = 0$), Eqs. (4b) and (5b) reduce to

$$\hbar k_\parallel = 0 \quad (6)$$

and

$$\hbar k_\perp = [2m(E_i + e\Phi - E_0)]^{1/2} . \quad (7)$$

B. Photoemission final states

We give a brief explanation for the use of Eq. (1), which we find to be generally applicable for GaAs and other materials[13,17] at photon energies of $25 \lesssim h\nu \lesssim 100$ eV. The final state for photoemission is just the time-reversed low-energy electron diffraction (LEED) state[22] which consists of a linear combination of plane waves outside the crystal, Bloch states inside the crystal, and surface evanescent states. It has been shown by Feibelman and Eastman[22] that the probability for photoemission is governed by the electric-dipole matrix element between the initial-valence Bloch state and the final time-reversed LEED state. The problem can be simplified in the limit of weak final-state momentum broadening and can be represented by the approximately equivalent three-step process: photoexcitation of the electron into excited Bloch states, transport to the surface, and emission from the surface. Here we assume that surface-evanescent final states can be neglected. The central and difficult problems are then the evaluation of the final Bloch states and the transmission coefficients of the final Bloch states through the surface. A detailed theoretical calculation of the latter is rather involved[12,23]; here we will confine ourselves to a qualitative discussion and consider a simple photoemission geometry, i.e., normal emission. The generalization to other geometries is straightforward.

For normal emission, the only plane-wave component detected outside the crystal has the form $\exp(ik'_\perp \xi)$ where ξ is the coordinate along the surface normal and $k'_\perp$ is the electron wave vector outside the crystal. Only Bloch states with significant Fourier components of the form $\exp(ik_\perp \xi)$ can couple well to $\exp(ik'_\perp \xi)$ outside the crystal. Energy must be conserved during transmission with additional momentum $\Delta k_\perp = k'_\perp - k_\perp$ supplied by the surface. Other Bloch states at the same energy, consisting mainly of Fourier components moving along directions other than the surface normal ($k_\parallel \neq 0$), are expected to have small coupling coefficients only via small plane-wave components normal to the surface and weak umklapp processes. Figure 1 shows such an analysis for the final states for normal emission along the [110] or Γ-K-X direction based on the nonlocal pseudopotential calculation given by Pandey[16] for GaAs. In the calculated energy range up to about 80 eV above E_v, there are about 100 energy bands all together. At momentum intervals of $\frac{1}{8}$ of the ΓKX distance along the [110] direction, all the wave functions have been Fourier analyzed and sorted according to the magnitude of the Fourier coefficient C of the term $\exp(ik_\perp \xi)$ using three intensity levels as shown in Fig. 1. The solid curve is the free-electron parabola ($k_\parallel = 0$ for normal emission)

$$E_f(k_\perp) = \hbar^2 k_\perp^2/2m + E_0 , \quad (8)$$

given by Eq. (1). The important final states with

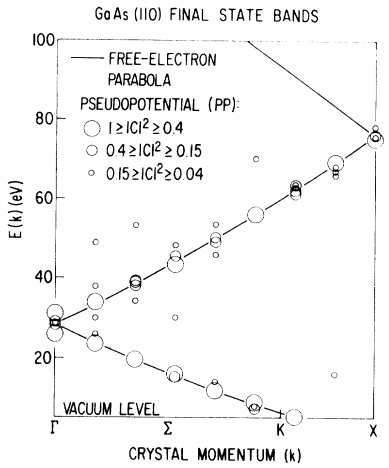

FIG. 1. Important final states for normal emission from GaAs (110). The final states are obtained from a pseudopotential calculation; they are sorted according to the Fourier coefficients and are shown for momentum intervals of $\frac{1}{8}$ of the ΓKX distance along [110]. The vertical scale is referenced to the valence-band maximum. See text for details.

significant Fourier coefficients C can be described quite well by this free-electron parabola. The deviation is typically $\lesssim 1$ eV at general $\vec{k}$ points and $\lesssim 5$ eV at zone center and boundaries. This behavior is expected since pseudopotential form factors are typically $\lesssim 3$ eV; Fig. 1 simply provides a clear visual display of the crowdedness of the final states in the reduced zone scheme and the bunching near the free-electron parabola. As will be shown in Sec. V, the energy broadening of the final states is typically 3–8 eV for energies of ~25–100 eV, hence we can simply consider the important final states as lying on a broadened free-electron parabola described by Eq. (8), or Eq. (1) in the general case. This is just the primary cone described by Mahan,[15] and these states should account for the predominant spectral peaks.

Bloch states which consist mainly of Fourier components moving in directions other than the surface normal and/or states which couple mainly through the surface umklapp process contribute generally less to the photoemission intensity. Emission due to these states is called secondary cone-surface umklapp emission.[23] A simple analysis shows that many Bloch states contribute to these processes. Due to lifetime broadening, the contributing states are smeared out to form more or less a continuum in the E-vs-$k_\perp$ space. Therefore, these processes result in nondispersive peaks in the spectra which reflect valence-band one-dimensional critical points with high state densities along the surface normal. The intensities of these secondary cone-surface umklapp emission peaks are typically an order of magnitude less than those of the primary cone peaks. We emphasize that the secondary cone-surface umklapp emission process is still direct transition in nature (with lifetime-broadened Bloch states), although the spectra would be similar to those predicted by an indirect-transition model.[9-12]

Note that the above argument is valid only at higher photon energies ($h\nu \gtrsim 25$ eV). At lower energies, the crystal potential as measured by the pseudopotential form factors is no longer a small perturbation, and final-state lifetime broadening becomes small. Consequently, detailed final-state dispersions are required for a full understanding of the photoemission spectra.[11] This behavior implies that photoemission spectra together with suitable band models and analyses can be used to determine final-state band dispersions, critical points, etc., if valence-band dispersions are well known.[11,23]

Other surface-related photoemission phenomena should also be considered. Emission from occupied surface states have been extensively studied for GaAs.[24] Emission via final evanescent states is also possible.[2,25] With a known band topology, it is generally not difficult to distinguish spectral peaks due to different emission processes. In the spectra to be presented below, emission due to occupied surface states and evanescent final states is unimportant due to the particular choices of $h\nu$, emission angles, and polarization.

IV. RESULTS AND DISCUSSION

A. Normal emission

Angle-resolved normal-emission spectra from the (110) surface are shown in Fig. 2, with the initial-state energy E_i referenced to the valence-band maximum E_v. E_v was determined by the Ga $3d_{5/2}$ core-level peak position (not shown) and its known binding energy of 18.6 eV.[26] Dashed and dotted curves connect peaks which are due to primary cone and secondary cone-surface umklapp emission from the valence bands, respectively (see below). Broad features A and A' are due to Ga and As $M_{4,5}VV$ Auger transitions, respectively.

The prominent peaks 1–4 in Fig. 2 show significant dispersion with changing $h\nu$. This behavior is consistent with the direct-transition model and inconsistent with the indirect-transition model. Therefore, we conclude that the direct-transition model is the correct model to be used. From the results to be presented below and discussion given in Sec. III, it is evident that peaks 1–4 are primary-cone-emission peaks. Using measured values of E_i and Eqs. (6) and (7), experimental band dispersions $E_i(\vec{k})$ have been directly deter-

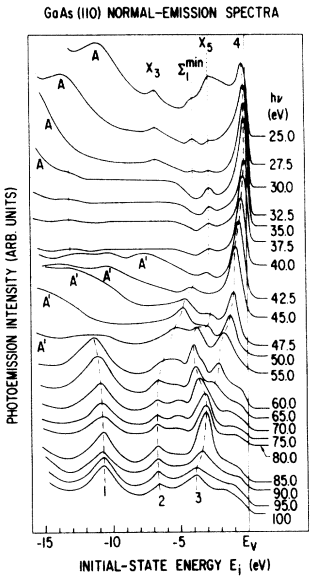

FIG. 2. Normal-emission angle-resolved energy-distribution curves from GaAs (110) surface as a function of photon energy $h\nu$. Dashed and dotted curves indicate peaks due to primary cone emission and secondary cone-surface umklapp emission, respectively. Structures A and A' are due to Ga and As $M_{4,5}VV$ Auger transitions, respectively. Energies are referenced to the valence-band maximum E_v.

mined along Γ-K-X and are summarized in Fig. 3. Data points (circles) obtained from peaks 1–4 in Fig. 2 correspond to transitions from valence-bands 1–4, respectively, with band 1 being the s-band. Dashed curves in Fig. 3 are calculated band dispersions based on a nonlocal pseudopoten-

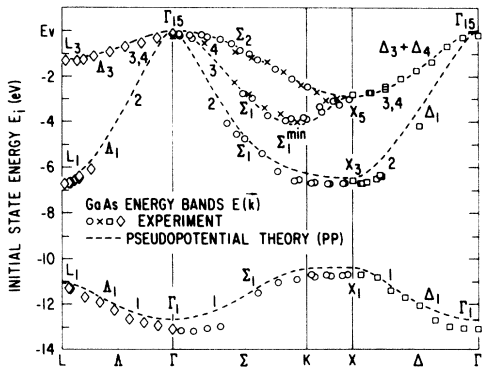

FIG. 3. Valence-band dispersions $E(\vec{k})$ of GaAs along major symmetry directions. Circles are experimental points obtained from normal emission spectra; crosses, squares, and diamonds are experimental points obtained from off-normal-emission spectra. Dashed curves are theoretical dispersion curves for valence bands 1–4 from Ref. 16. The symmetry characters of the bands and the critical points are labeled.

tial theory which was fit to angle-integrated photoemission data.[16] The agreement is very good. The spin-orbit interaction for GaAs, which has been neglected in the theoretical calculation, is quite small and does not show up directly in the spectra. The largest splitting occurs at the Γ_{15} point (0.35 eV)[27] and transitions from these split states give rise to a single broad, asymmetric peak at about 0.15 eV below E_v as observed experimentally ($h\nu \simeq 30$ eV, Fig. 2).[28] Elsewhere, the splitting is typically much less than 0.2 eV, out best experimental resolution, and the peak positions observed in Fig. 2 simply reflect the average band dispersions.

Since E_f and E_i in Eqs. (1) and (2) are lifetime broadened by about 3–8 eV and 0–2 eV (see Secs. III and V), respectively, this leads to an uncertainty in $k_\perp$, typically $\lesssim 0.1\ \Gamma KX$ for the data points shown in Fig. 3. The finite angular resolution $\Delta\theta = 4°$ also leads to uncertainty in $\vec{k}_\parallel$ and thus uncertainty in E_i; the effect is large for band dispersions $E_i(\vec{k})$ with large curvature. It is estimated from Fig. 3 and Eq. (4) that $\Delta E_i \simeq 0.2$ eV near the X_5 critical point due to this effect, and much smaller elsewhere for the results in Fig. 3.

The behavior of the primary cone peaks 1–4 in Fig. 2 can now be readily understood in terms of the broadened free-electron dispersion for the final states. As $h\nu$ increases, peak 4 moves through a maximum energy position corresponding to the Γ_{15} critical point at $h\nu \simeq 30$ eV and turns back, while peak 3 moves through a minimum ($\Sigma_1^{\min}$) at $h\nu \simeq 65$ eV, peaks 3 and 4 subsequently coalesce for $h\nu \simeq 80$ eV, i.e., at the X_5 critical point, and finally peak 3 moves back near $\Sigma_1^{\min}$ at $h\nu \simeq 100$ eV, and so on. The various turning points of the peaks mark the Brillouin-zone center and boundary crossings and can be used to determine an experimental value for E_0 in Eq. (1) and to check the validity of the nearly-free-electron final-state dispersion. For example, the extremal position of peak 4 at $E_1 \simeq -0.15$ eV for $h\nu \simeq 30$ eV corresponds to the transition at the zone center with

$$k_\perp = 2\left(2\frac{\pi}{a}\sqrt{2}\right) = 2\Gamma KX, \tag{9a}$$

in the extended-zone scheme, and

$$(k_\perp)_{\text{red}} = 0, \tag{9b}$$

in the reduced-zone scheme. Using Eq. (7), we obtain the experimental value of $E_0 \simeq -8$ eV compared to the theoretical value of -9.34 eV. The agreement is quite good considering the fact that E_f in Eqs. (1) and (2) is uncertain by about 5 eV due to lifetime broadening. Furthermore, using the experimentally determined photothreshold $e\Phi = 5.15$ eV we obtain the experimental value for the

inner potential $V_0 = E_0 - e\Phi \simeq -13$ eV, in good agreement with LEED results.[29] The nondispersive peaks labeled X_3, $\Sigma_1^{\min}$, and X_5 in Fig. 2 are secondary cone-surface umklapp emission peaks associated with the corresponding critical points in Fig. 3. Their peak positions give directly the energies of the critical points. We therefore obtain an accurate set of critical point energies at Γ and X by using the experimental $E(\vec{k})$ dispersions in Fig. 3 and those determined from secondary cone-surface umklapp peaks. The results are collected in Table I (to be discussed).

B. Off-normal emission

We describe a simple off-normal-emission technique to determine the valence-band dispersions $E_i(\vec{k})$ in the high-symmetry $[\bar{1}10](\Gamma\text{-}K\text{-}X)$, $[00\bar{1}](\Gamma\text{-}\Delta\text{-}X)$, and $[\bar{1}1\bar{1}](\Gamma\text{-}\Lambda\text{-}L)$ directions using the same cleaved GaAs (110) surface. It is also feasible to use the normal-emission technique described previously for this purpose provided crystal faces of appropriate orientations are prepared. However, this involves the preparation of additional crystal surfaces and is more involved experimentally since the {100} and {111} faces cannot be obtained by simple cleavage.

We will concentrate on the primary-cone-emission peaks, since these are relatively intense and usually can be easily recognized and measured. To determine the band dispersions $E_i(\vec{k})$ along any one of three major symmetry directions $[\bar{1}10]$, $[00\bar{1}]$, and $[\bar{1}1\bar{1}]$ parallel to the surface, $\vec{k}_\parallel$ is chosen to lie along the desired direction with suitable azimuthal emission angle. For each polar emission angle θ, $h\nu$ is adjusted according to Eq. (5b) such that $k_\perp = 2\Gamma KX$ or $(k_\perp)_{\rm red} = 0$ [cf. Eq. (9)], that is, $(\vec{k})_{\rm red} = \vec{k}_\parallel$ is now along the desired symmetry direction.[30] By scanning θ while adjusting $h\nu$ accordingly, the band dispersions $E_i(\vec{k})$ are obtained simply from the measured values of E_i and Eq. (4b). Since E_f (or equivalently $k_\perp$) in Eq. (1) is broadened, $h\nu$ need not be set exactly. Furthermore, since the band dispersions are stationary (zero slope) when $k_\perp = 2\Gamma KX$, a small deviation of $k_\perp$ from $2\Gamma KX$ resulting from a small deviation of $h\nu$ has little effect on the measured value of E_i. In the results presented below, the maximum deviation of $k_\perp$ from $2\Gamma KX$ is less than 5%; the effect is indeed small ($\Delta E_i \lesssim 0.1$ eV) from an examination of the band dispersions $E_i(\vec{k})$ shown in Fig. 3. Finite angular resolution introduces uncertainty in $\vec{k}_\parallel$ leading to $\Delta k_\parallel \simeq 0.1\ \Gamma KX$ and $\Delta E_i \lesssim 0.1$ eV.

Off-normal emission spectra with $\vec{k}_\parallel \| [\bar{1}10](\Gamma\text{-}K\text{-}X)$ recorded according to the above prescription for $h\nu$ are shown in Fig. 4. Primary-cone-emission peaks 3 and 4 derived from bands 3 and 4 are indicated by dashed lines; their behaviors are very similar to those found in Fig. 2. Experimental $E_i(\vec{k})$ determined from these spectra are shown as crosses in Fig. 3. The agreement with the normal-emission data along [110] (circles) is excellent and confirms our technique.

The data with $\vec{k}_\parallel \| [00\bar{1}](\Gamma\text{-}\Delta\text{-}X)$ and $\vec{k}_\parallel \| [\bar{1}1\bar{1}]$

TABLE I. Left columns: experimental and theoretical valence critical-point energies referenced to the valence-band maximum. Right column: experimental inverse lifetimes at the valence critical points.

Method	Valence critical-point energy (eV) ARPES[a]	XPS[b]	NEPM[c]	NEPM[d]	ROPW[e]	Inverse lifetime (eV) ARPES[a]
Γ_{15}^V	0	0	0	0	0	
Γ_1^V	−13.1	−13.8	−12.67	−12.55	−12.4	2.0
L_3^V	−1.30	−1.4	−1.24	−1.31	−1.1	0.8
L_1^V	−6.70	−7.1	−6.48	−6.83	−6.4	1.0
L_1^V	−11.24	−12.0	−11.07	−10.60	−10.9	2.0
X_5^V	−2.80	−2.5	−2.86	−2.95	−2.4	0.9
X_3^V	−6.70	−7.1	−6.46	−6.88	−6.4	1.4
X_1^V	−10.75	−10.7	−10.40	−9.83	−10.2	2.0
$\Sigma_1^{\min}$	−4.0	−4.4	−4.13	−4.3		0.6

[a] Angle-resolved photoelectron spectroscopy, this work.
[b] X-ray photoelectron spectroscopy, Ref. 33.
[c] Nonlocal empirical pseudopotential method, Ref. 16.
[d] Nonlocal empirical pseudopotential method, Ref. 27.
[e] Relativistic OPW, Ref. 34.

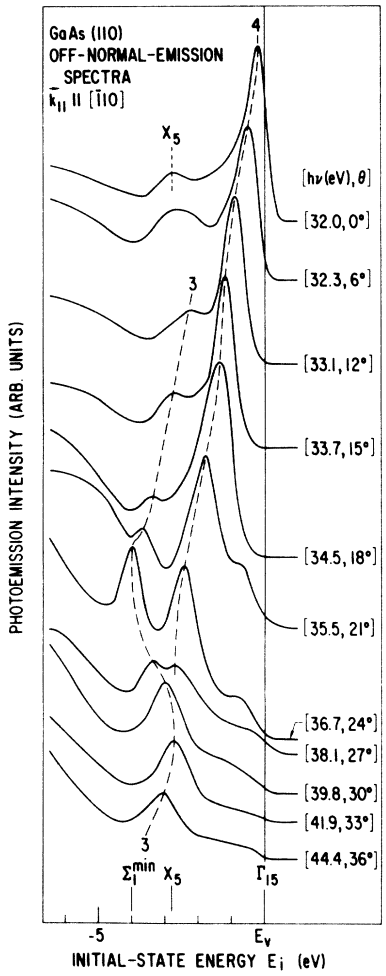

FIG. 4. Off-normal-emission spectra from GaAs (110) for $\vec{k}_{\parallel} \| [\bar{1}10]$ and $k_\perp = 2\Gamma KX$ held fixed. The photon energy $h\nu$ and polar emission angle θ are indicated and correspond to $k_{\parallel}$ varying from $k_{\parallel} = 0$ (top curve) to $k_{\parallel} = 1.15$ ΓKX (bottom curve). Dashed curves and dotted curves indicate peaks due to primary cone emission and secondary cone-surface umklapp emission, respectively. Relevant valence critical points are indicated near the bottom of the figure.

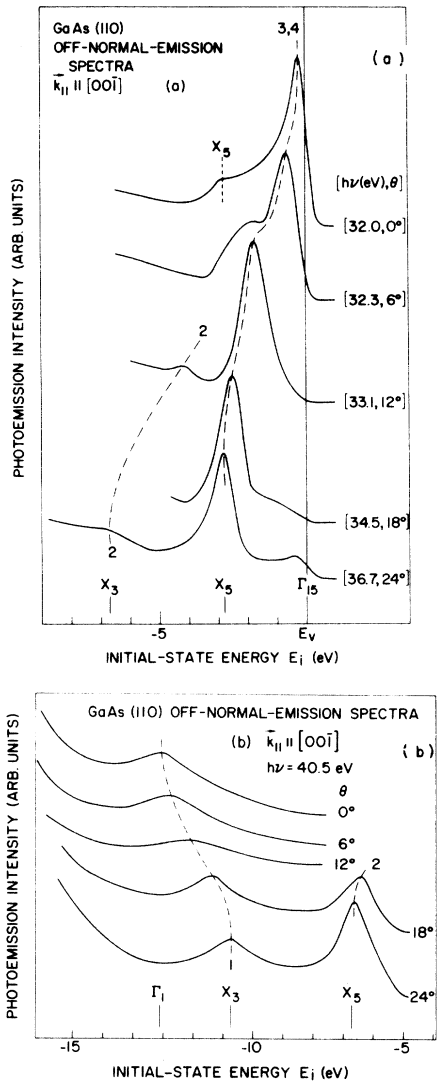

FIGS. 5(a), (b). Off-normal-emission spectra from GaAs (110) with $\vec{k}_{\parallel} \| [00\bar{1}]$ and $k_\perp = 2\Gamma KX$ held fixed. The photon energy $h\nu$ and polar emission angle θ are indicated and correspond to $k_{\parallel}$ varying from $k_{\parallel} = 0$ (top curve) to $k_{\parallel} \simeq \Gamma\Delta X$ (bottom curve). Dashed curves and dotted curves indicate peaks due to primary cone emission and secondary cone-surface umklapp emission, respectively. Relevant valence critical points are indicated near the bottom of the figures.

$\times(\Gamma\text{-}\Lambda\text{-}L)$ are very similar. Some typical spectra are shown in Figs. 5 and 6. Due to the wide spread of E_i, different $h\nu$'s were used for different energy regions so as to hold $k_\perp \simeq 2\Gamma KX$. Some spectra were truncated to eliminate confusion due to strong core-level emission from the second-order light from our monochromator. A fixed $h\nu = 40.5$ eV was used in Figs. 5(b) and 6(b), although the optimum value should be higher according to Eq. (5b). This was done to avoid the As $M_{4,5}VV$ Auger emission (see Fig. 2). The experimental $E_i(\vec{k})$ are shown as squares and diamonds in Fig. 3 together with the theoretical band dispersions[16] (dashed curves). Note in particular $E_i(\vec{k})$ at the X point obtained from measurements along $\Gamma\text{-}K\text{-}X$ and $\Gamma\text{-}\Delta\text{-}X$ agree very well; this further confirms our techniques. Experimental critical point energies at L are listed in Table I.

V. ELECTRON AND HOLE LIFETIMES

In the direct-transition model, an electron is photoexcited to a final Bloch state leaving a hole in the initial Bloch state. The photoelectron dis-

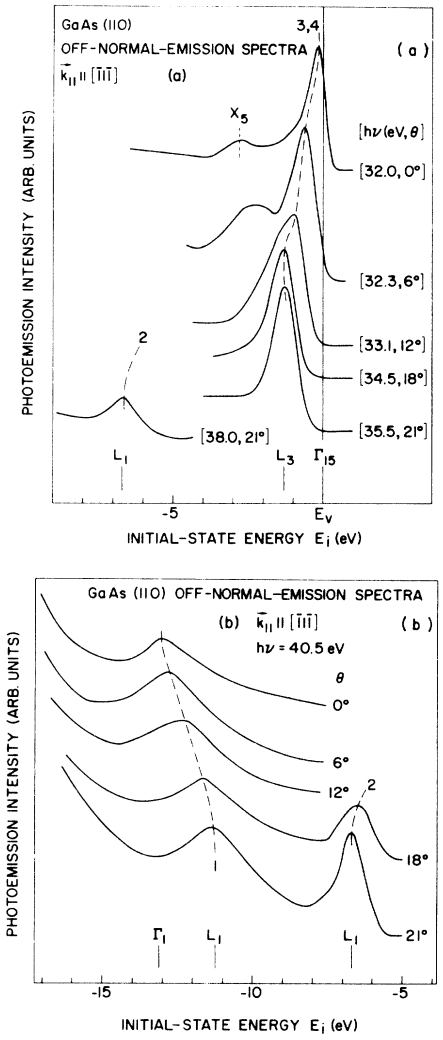

FIGS. 6(a), (b). Same as Figs. 5(a) and 5(b) except for $\vec{k}_{\parallel} \parallel [\bar{1}1\bar{1}]$, and $k_{\parallel}$ varying from $k_{\parallel} = 0$ (top curve) to $k_{\parallel} \simeq \Gamma\Delta L$ (bottom curve).

tribution of a given transition is given by a golden-rule-type formula

$$D(E_f) \propto \int |M|^2 S_i(E_i, \vec{k}_i) S_f(E_f, \vec{k}_f) \times \delta_{\vec{k}_i \vec{k}_f} \delta(E_f - E_i - h\nu) f(\theta, \phi) d\vec{k}_i \, d\vec{k}_f \, dE_i \,, \tag{10}$$

where M is the appropriate dipole matrix element, $f(\theta, \phi)$ is the angular collection function of the analyzer, and S_i and S_f are the hole and electron spectral distribution functions, respectively, given by

$$S_{i,f}(E, \vec{k}) \propto \frac{\Gamma_{h,e}(\vec{k})}{[E - E_{i,f}(\vec{k})]^2 + [\Gamma_{h,e}(\vec{k})/2]^2} \,, \tag{11}$$

with Γ_h and Γ_e being the hole and electron inverse lifetimes, respectively. Assuming $|M|^2$ is a constant in the region of interest, and $f(\theta, \phi)$ is infinitely sharp, we obtain to first order that $D(E_f)$ has a Lorentzian line shape with a width given by

$$\Gamma = \left| \frac{\Gamma_h + \left| \frac{V_{h\perp}}{V_{e\perp}} \right| \Gamma_e}{1 - \frac{V_{h\perp}}{V_{e\perp}} - \frac{m V_{h\perp}}{\hbar k_{\parallel}} \sin^2\theta + \frac{V_{h\perp}}{V_{e\perp}} \frac{m V_{e\parallel}}{\hbar k_{\parallel}} \sin^2\theta} \right| , \tag{12}$$

where $V_{h\parallel}$, $V_{h\perp}$, $V_{e\parallel}$, and $V_{e\perp}$ are the parallel and perpendicular components of the hole and electron group velocities, respectively, and $k_{\parallel}$ is defined in the extended zone. The hole and electron group velocities can be calculated using the experimental $E_i(\vec{k})$ in Fig. 3 and Eq. (1), respectively. Second- and higher-order derivatives of E vs $\vec{k}$ and first-order changes of $\Gamma_{e,h}(\vec{k})$ have been neglected in Eq. (12); this is not justified in general, and a useful rule for testing the validity of Eq. (12) is given by

$$|\nabla_k \hbar V_{h,e}| \ll (\hbar V_e)^2 / \Gamma \tag{13a}$$

and

$$|\nabla_k \Gamma_{h,e}(\vec{k})| \ll \hbar V_e \,. \tag{13b}$$

For normal emission, Eq. (12) is simplified to yield[2,7,31,32]

$$\Gamma_N = \left| \frac{\Gamma_h + |R_\perp| \Gamma_e}{1 - R_\perp} \right| , \tag{14}$$

where $R_\perp = V_{h\perp}/V_{e\perp}$. For off-normal emission but with $k_\perp = 2\Gamma KX$ as we have used, Eq. (12) simplifies to

$$\Gamma_0 = \left| \frac{\Gamma_h}{1 - (m V_{h\parallel}/\hbar k_{\parallel}) \sin^2\theta} \right| . \tag{15}$$

With finite but small angular resolution, the line width and line shape are not changed for normal emission to first order since

$$[\partial E_i(k_{\parallel}, k_\perp)/\partial k_{\parallel}]_{k_{\parallel}=0} = 0. \tag{16}$$

With our experimental parameters and 4° angular resolution, the line shape for off-normal emission is still very close to a Lorentzian with a width Γ_0' given by

$$\Gamma_0'^2 = \Gamma_0^2 + \left(\frac{(\cot\theta) \hbar k_{\parallel} V_{h\parallel}}{1 - (m V_{h\parallel}/\hbar k_{\parallel}) \sin\theta} \Delta\theta \right)^2 , \tag{17}$$

where Γ_0 is given by Eq. (15) and $\Delta\theta = 4° = 0.07$ radian. Note Γ_0' is independent of Γ_e while Γ_N depends on both Γ_h and Γ_e. Since the matrix element is in general not a constant, and higher-order effects may not always be negligible, the line shapes observed in the spectra are not necessarily Lorentzian. Bearing in mind the limitations,

Eqs. (14) and (17) can be used to extract lifetime information.

Peaks derived from band 1 in Figs. 5(b) and 6(b) (peaks 1) are relatively broad and well separated from other peaks. From measured line widths and Eq. (17), $\Gamma_h(\vec{k})$ can be easily determined. Within experimental uncertainty and the limitations mentioned above, $\Gamma_h(\vec{k}) = 2.0$ eV = constant for band 1 along Γ-Δ-X and Γ-Λ-L. It is therefore reasonable to assume $\Gamma_h(\vec{k}) = 2.0$ eV independent of $\vec{k}$ for band 1. This is physically plausible because the dominant decay mechanism for a band 1 hole is the Auger decay and is determined mainly by the available phase space, which is nearly constant.

Using the normal-emission line width of peak 1 in Fig. 2 and Eq. (14), the electron inverse lifetime Γ_e can be obtained with Γ_h set equal to 2.0 eV. In Fig. 2, the width of peak 1 varies from 2.0 eV at $\Gamma_1(h\nu \sim 40$ eV), to ~2.8 eV at $\sim\frac{1}{2}(\Gamma KX)$ ($h\nu \sim 60$ eV), to 2.0 eV at $X_1(h\nu \sim 85$ eV). At $\frac{1}{2}(\Gamma KX)$, using Eq. (14), we obtain $\Gamma_e \simeq 5$ eV for an electron state at ~50 eV above E_v. The corresponding electron mean free path, or escape depth is calculated using Eq. (8) to be ~6 Å, in agreement with previous estimates based on overlayer methods.[18] This escape depth corresponds to an electron momentum uncertainty of less than 10% of ΓKX, consistent with a direct-transition model.

The analysis for peaks 2–4 are similar but more difficult due to overlapping of spectral peaks and background effects. They are relatively narrow and instrumental resolution has to be considered. The experimental inverse lifetimes for valence critical points are included in Table I. The measured values are generally larger than previous estimates.[33]

VI. CONCLUSIONS

Table I summarizes our experimentally determined valence critical-point energies obtained from $E_i(\vec{k})$ in Fig. 3 and secondary cone surface umklapp emission peaks, together with values from other experimental and theoretical results.[16,27,33,34] As seen in Table I, theoretical values based on past data generally show good agreement, with errors ranging from ~0 to 0.5 eV. Using the optical transition energies measured by reflectivity,[35] we also compile a list of low-lying conduction-band critical-point energies in Table II. Although the reflectivity measurements were performed at liquid-He temperature and our measurements were performed at room temperature, the observed rigidity of the valence bands with temperature[36] implies that the values in Table II should be regarded as liquid-He temperature values. The small spin-orbit splittings (<0.2 eV)[27] have been neglected. The experimental valence-band and conduction band critical-points in Tables I and II should provide a basis for refined theoretical models of GaAs.

TABLE II. Experimental and theoretical low-lying conduction-band critical-point energies referred to the valence-band maximum.

	Conduction critical-point energy (eV)		
Method	Expt.[a]	NEPM[b]	NEPM[c]
Γ_1^c	8.33	8.14	
Γ_{15}^c	4.716	4.62	4.63
Γ_1^c	1.632	1.62	1.51
L_1^c	1.85	1.91	1.82
X_3^c	2.58	2.45	2.38
X_1^c	2.18	2.06	2.03

[a] Obtained using the valence critical-point energies from this work and optical transition energies from Ref. 35. These energies are for He temperature and referred to the valence-band maximum. Spin-orbit splittings are neglected.

[b] Nonlocal empirical pseudopotential method, Ref. 16.

[c] Nonlocal empirical pseudopotential method, Ref. 27.

The direct-transition model and the techniques described in this paper should be applicable to many other materials[14,17] and to higher photon energies. The final-state lifetime broadening becomes large at higher photon energies, but the dispersion of the free-electron-like primary cone increases much faster. Therefore $k_\perp$ uncertainty becomes smaller and a more accurate determination of $E_i(\vec{k})$ can be achieved as $h\nu$ increases above ~100–200 eV. Moreover, a measurement of $\Gamma_e(E_f)$ over a wide energy range should be interesting theoretically. With the rapid development in technology and instrumentation, such experiments should become feasible in the near future, despite more stringent experimental requirements (such as better angular resolution).

ACKNOWLEDGMENTS

We acknowledge the help of K. C. Pandey, F. Himpsel, E. Dietz, J. F. van der Veen, J. J. Donelon, A. Marx, and E. Rowe and the staff of the Physical Sciences Laboratory. One of us (T.-C.C.) wishes to express his appreciation to D. E. Aspnes for useful conversations. This work is supported in part by the U. S. Air Force Office of Scientific Research, Contract No. F44620-76-C-0041.

*Present address: Sandia Laboratories, Albuquerque, New Mexico 87185.

†Present address: Physical Sciences Laboratory, University of Wisconsin-Madison, Stoughton, Wisconsin 53589. Permanent address: National Institute for Research in Inorganic Materials, Sakura, Niihari, Ibaraki 300-31, Japan.

[1]See, for example, *Topics in Applied Physics*, Vol. 26, edited by L. Ley and M. Cardona (Springer-Verlag, Berlin, 1979), pp. 237–264.

[2]P. Thiry, D. Chandesris, J. Lecante, C. Guillot, R. Pinchaux, and Y. Petroff, Phys. Rev. Lett. 43, 82 (1979).

[3]L. F. Wagner, Z. Hussain, and C. S. Fadley, Solid State Commun. 21, 257 (1977).

[4]J. Stohr, P. S. Wehner, R. S. Williams, G. Apai, and D. A. Shirley, Phys. Rev. B 17, 587 (1978).

[5]S. P. Weeks and J. E. Rowe, Solid State Commun. 27, 885 (1978).

[6]F. J. Himpsel, J. A. Knapp, and D. E. Eastman, Phys. Rev. B 19, 2919 (1979); D. E. Eastman, F. J. Himpsel, and J. A. Knapp, Phys. Rev. Lett. 40, 1514 (1978).

[7]J. A. Knapp, F. J. Himpsel, and D. E. Eastman, Phys. Rev. B 19, 4952 (1979).

[8]E. Dietz and D. E. Eastman, Phys. Rev. Lett. 41, 1674 (1978).

[9]T. Grandke, L. Ley, and M. Cardona, Phys. Rev. Lett. 38, 1033 (1977); Solid State Commun. 23, 897 (1977).

[10]P. Thiry, R. Pinchaux, G. Martinez, Y. Petroff, J. Lecante, J. Paigne, Y. Ballu, C. Guillot, and D. Spanjaard, Solid State Commun. 27, 99 (1978).

[11]K. A. Mills, D. Denley, P. Perfetti, and D. Shirley, Solid State Commun. 30, 743 (1979).

[12]T. Grandke, L. Ley, and M. Cardona, Phys. Rev. B 18, 3847 (1978).

[13]T. -C. Chiang, J. A. Knapp, D. E. Eastman, and M. Aono, Solid State Commun. 31, 917 (1979).

[14]M. Aono, T. -C. Chiang, J. A. Knapp, and D. E. Eastman, Solid State Commun., in press (1979).

[15]G. D. Mahan, Phys. Rev. B 2, 4334 (1970).

[16]K. C. Pandey (unpublished); K. C. Pandey and J. C. Phillips, Phys. Rev. B 9, 1552 (1974).

[17]T.-C. Chiang and D. E. Eastman, Phys. Rev. B (to be published).

[18]P. Pianetta, I. Lindau, C. M. Garner, and W. E. Spicer, Phys. Rev. B 18, 2792 (1978).

[19]See, for example, C. Kittel, *Quantum Theory of Solids*, (Wiley, New York, 1963), p. 213.

[20]J. Hermanson, Solid State Commun. 22, 9 (1977).

[21]R. H. Parmenter, Phys. Rev. 100, 573 (1955).

[22]P. J. Feibelman and D. E. Eastman, Phys. Rev. B 10, 4932 (1974).

[23]D. E. Eastman, F. J. Himpsel, J. A. Knapp, and K. C. Pandey, Inst. Phys. Conf. Ser. 43, 1059 (1979).

[24]J. A. Knapp, D. E. Eastman, K. C. Pandey, and F. Patella, J. Vac. Sci. Technol. 15(4), 1252 (1978).

[25]E. Dietz and F. J. Himpsel, Solid State Commun. 30, 235 (1979).

[26]W. Gudat and D. E. Eastman, J. Vac. Sci. Technol. 13, 831 (1976).

[27]J. R. Chelikowsky and M. L. Cohen, Phys. Rev. B 14, 556 (1976).

[28]Similar experimental results for GaSb (Ref. 17) clearly show the spin-orbit splitting at Γ_{15}(~0.8 eV). Transitions due to the two components are of comparable intensity.

[29]A. Kahn, E. So, P. Mark, C. B. Duke, and P. J. Meyer, J. Vac. Sci. Technol. 15, 1223 (1978).

[30]Other convenient values of $k_\perp$ can also be used. See for example, Ref. 14.

[31]J. B. Pendry, in *Photoemission and the Electronic Properties of Surfaces*, edited by Feuerbacher, Fitton, and Willis (Wiley, New York, 1978), p. 94.

[32]U. Gerhardt (private communications).

[33]L. Ley, R. A. Pollak, F. R. McFeely, S. R. Kowalczyk, and D. A. Shirley, Phys. Rev. B 19, 600 (1974).

[34]I. B. Ortenburger and W. E. Rudge, IBM Research Laboratory Report No. RJ-1041, 1972 (unpublished).

[35]D. E. Aspnes, C. G. Olson, and D. W. Lynch, Phys. Rev. B 12, 2527 (1975).

[36]D. Auvergne, J. Camassel, H. Mathieu, and M. Cardona, Phys. Rev. B 9, 5168 (1974).